Original Research

S. Garré
L. Pagès
E. Laloy
M. Javaux
J. Vanderborght*
H. Vereecken

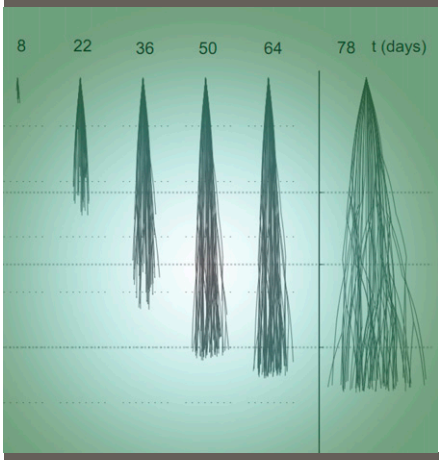

Plant water uptake models that use 3-D representations of root structures have been developed recently. These models require a 3-D root architecture as input. We investigated how the root architecture model RootTyp can be parameterized from observations of root arrival data at minirhizotron tube interfaces.

S. Garré, M. Javaux, J. Vanderborght, H. Vereecken, Forschungszentrum Jülich GmbH, Agrosphere (IBG-3), 52425 Jülich, Germany; S. Garré, Gembloux Agro-Bio Tech, Université de Liège (ULg), Passage des déportés 2, 5030 Gembloux, Belgium; M. Javaux, Earth and Life Institute/Environmental Sciences, Université catholique de Louvain (UCL), Croix du Sud 2, bte 2. 1348 Louvain-la-Neuve, Belgium; L. Pagès, Plantes et Systèmes de culture Horticoles, INRA PACA Avignon, UR 1115, Site Agroparc, 84914 Avignon Cedex 9, France; E. Laloy, Environment, Health and Safety, SCK-CEN, Boeretang 200, 2400 Mol, Belgium. *Corresponding author (jan.vanderborght@biw.kuleuven.be)

Vadose Zone J.
doi:10.2136/vzj2011.0179
Received 29 Nov. 2011.

Parameterizing a Dynamic Architectural Model of the Root System of Spring Barley from Minirhizotron Data

The development of models describing water and nutrient fluxes to and through 3-D spatially resolved root structures in soils brings along the need to predict or describe the root architecture and root growth in detail. However, detailed data to calibrate and validate such architecture and growth models is typically not available. Here, we investigate the sensitivity of the root architecture model RootTyp to changes in its model parameters and reconstructed the root system architecture of barley (*Hordeum vulgare* L.) growing in an undisturbed lysimeter using minirhizotron images at four different depths. Root arrival curves from a series of minirhizotron images were used to parameterize RootTyp using a range of realistic architectures. We adjusted a simple architecture to the data, which contained only long primary roots starting from the seed. This simple model unfortunately could not reproduce the observed increase of root density with depth. The model was subsequently improved by allowing root branching and elongation to be horizon-dependent and by making reiteration of root tips possible. Reiteration is an alternative form of branching, where secondary roots can become as long and thick as primary roots. Our results show that minirhizotron data do not contain enough information to warrant identification of the parameters governing these processes, as the additional parameters act similarly on data characteristics as the initial ones. Therefore, different experimental techniques should be combined to constrain the model parameters better in the future.

Abbreviations: DOY, day of the year; EE, elementary effect; MRI, magnetic resonance imaging; NMR, nuclear magnetic resonance; PVC, poly-vinyl chloride; SLP, the slope of the arrival curve between t20% and t80% (d^{-1}); RS, root system.

A plant's root system (RS) provides anchorage and allows the plant to acquire water and nutrients. Characterizing the three-dimensional architecture of this RS remains a challenging task. In an undisturbed soil, it is virtually impossible to assess the three-dimensional root system architecture of mature plants without actually destroying it. During the past decades, novel geophysical methods have been explored for the purpose of root architecture mapping, such as X-ray tomography (e.g., Tracy et al., 2010), neutron radiography (e.g., Willatt et al., 1978; Menon et al., 2007; Moradi et al., 2009), and nuclear magnetic resonance (NMR) (Pohlmeier et al., 2008). However, these techniques are restricted to small soil cores (with limited length or width), to single plants, and often, limited to certain soil types. As such, it is still unfeasible to monitor root growth non-invasively and study soil-plant interactions in a natural environment. Additional difficulties arise with the presence of plant roots from multiple different species. One option might be to use experimental datasets, providing partial information on the RS, together with existing 3-D root architecture models to reconstruct plausible RS architectures by inverse optimization.

The first mechanistic RS architecture models were introduced in the early 1970s in the pioneering work of Hackett and Rose (1972). The ever increasing pace of computational power, has stimulated the development of increasingly complex plant architectural models (Diggle, 1988; Pagès et al., 1989; Clausnitzer and Hopmans, 1994; Lynch et al., 1997; Somma et al., 1998; Wu et al., 2007). Most available root models, conceptualize the RS architecture as a complex cipher structure describing the geometrical properties of the different roots and the topology of their connections (Dupuy et al., 2010a). These models provide good explicit descriptions and visualization of the RS, but at the expense of many unknown parameters whose values are typically difficult to obtain directly in practice. Indeed, de Willigen et al. (2002) developed analytical solutions for root growth in soil as a 2-D diffusion process, which substantially reduces the dimensionality of the parameter space.

Most techniques used to obtain partial information on the RS architecture are extremely time-consuming and thus expensive. Typical traditional techniques in field soils are soil cores, observation of trench walls, in growth cores and root excavation [see Smit et al. (2000) for more information on sampling strategies]. Today, minirhizotrons are the only practical method to assess root system dynamics in large lysimeters or field soils. Minirhizotrons are clear glass or plastic tubes, installed in the soil under the plants. The tubes can be installed in an undisturbed soil by augering or in a container or pit filled with repacked soil. An endoscope is used to make pictures of the roots growing along the outside walls of the tubes. By making repeated images through time, the progress of the roots can be followed as they appear, mature and die. However, rhizotubes represent only a portion of the rooted volume and, if they are installed horizontally, information is only available at some discrete depths. Moreover, it has been shown that a rhizotube surface may act as an altered environment for the roots, possibly changing root length and other architectural features (Bragg et al., 1983; Upchurch and Ritchie, 1983; Levan et al., 1987; McMichael and Taylor, 1987; Vos and Groenwold, 1987; Parker et al., 1991). Still, there is an important advantage of the minirhizotron technique: as opposed to destructive techniques, the method can be used to follow the evolution of the root arrival time in situ. Since root growth is not disturbed until the roots reach the rhizotube, the number of roots arriving at the rhizotube as a function of time at a certain depth contains reliable information on root growth (e.g., Parker et al., 1991; Smit et al., 2000). When these root arrival curves are assessed at several depths, they can be used to calibrate a RS architecture model. For example, Dupuy et al. (2010b) used this type of information to construct the root meristem density function for barley (*Hordeum vulgare L.*) in large, disturbed containers.

In this paper we will (i) explore the value of the information that can be extracted from root arrival curves detected in minirhizotron images in horizontally installed rhizotubes at four depths; (ii) assess the sensitivity of characteristics of root arrival curves to parameters of the RS model RootTyp (Pagès et al., 2004); and (iii) assess if the parameters of the model can be estimated from minirhizotron data and what information about the RS architecture they contain. We will use minirhizotron data from root growth of spring barley in two different lysimeters containing undisturbed soil monoliths of a silty soil.

Materials and Methods

Lysimeter Set-up

We excavated two undisturbed soil monoliths using a large polyvinyl chloride (PVC) column (height = 150 cm, inner diameter = 116 cm) from intensively used arable land near Merzenhausen (Germany). In the following, the lysimeters will be referred to as S1 and S2. These lysimeters where replications of the same soil and were part of a larger investigation (Garré, 2010; Garré et al., 2011) using ERT to monitor heterogeneous water uptake and solute transport in bare and cropped soil. To avoid soil compaction at the cylinder wall of the lysimeters, a cutting edge was made at the bottom of the PVC mantle and the soil below and outside of the lysimeter was excavated when the lysimeter was step by step pushed into the soil. The soil was classified as an orthic Luvisol (FAO/ISRIC/ISSS, 1998). Four soil horizons were identified: A_p (0–40 cm), B_t (41–70 cm), B_{v1} (71–100 cm), and B_{v2} (>100cm). Earthworm burrows were abundant down to more than 150 cm, although only few direct connections to the soil surface exist, because of frequent plowing (Burkhardt et al., 2005). Root channels were generally <10 mm (with the maximum diameter resulting from tap roots of sugar beet) and were found up to a depth of 1.2 m.

In the beginning of the experiment, the volumetric water content in the bare soil column varied with depth between 0.30 and 0.45 (Garré et al., 2011). In the bottom half of S1, there still was $CaCl_2$–tracer available in the pore water as a result of ongoing tracer transport investigations (Garré, 2010). Garré et al. (2011) used ERT to map the spatial variability of soil moisture in lysimeter S2. For S1, soil moisture variability could not be inferred from ERT measurements since these measurements depend on both the soil water content and the salinity of the soil solutions. However, since the lysimeters were taken from the same soil, it can be assumed that the within lysimeter variations in soil moisture were similar in both lysimeters. We sowed the spring barley (*Hordeum vulgare L.*) in parallel lines approximately 24 cm apart on DOY 132. We made small lines of approximately 2 cm deep, spread the barley seeds (ca. 0.6 seeds/cm) in these lines and covered them with soil. This experimental set-up was similar to the one of Dupuy et al. (2010b) apart from the fact that an undisturbed soil was studied in this research as opposed to the filled soil containers and there was a larger distance between the rhizotubes in this study than in the one of Dupuy et al. (2010b).

The soil did not receive any additional water until DOY 209. To estimate the plant density, the number of plants was counted just after emergence and at the end of the growing season using a picture of the lysimeter surface. In both lysimeters the photograph counts resulted in approximately 200 plants or 0.019 plants cm^{-2} (S1: 198, S2: 217). It must be noted that tillering of the barley makes the plant number difficult to quantify at later stages of development. This counting method is however accurate enough to get an estimate of the population density, allowing comparison with densities typical for agricultural practice. Figure 1 gives an overview of the experimental set-up.

Minirhizotron: Data Acquisition and Analysis

Four rhizotubes (T1-T4) were installed horizontally before sowing at the side of the lysimeter at −22.5/19.5, −47.5/44.5, −72.5/69.5 and −122.5/119.5 cm depth for S1/S2, respectively. The installation was performed after the lysimeter excavation using a home-made, steel soil auger with a diameter slightly smaller than the rhizotube outer diameter to avoid voids between tube and soil.

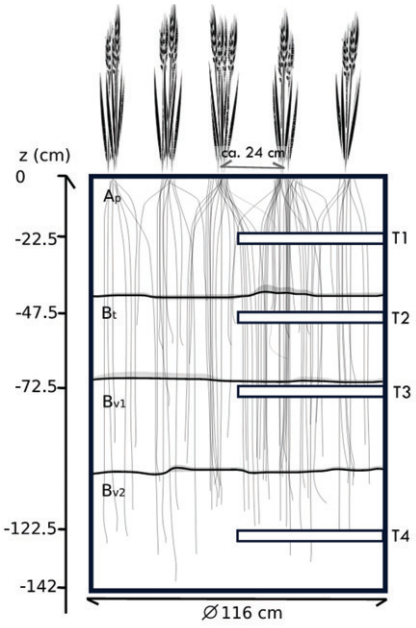

Fig. 1. Scheme of lysimeter set-up with barley (lysimeter S1).

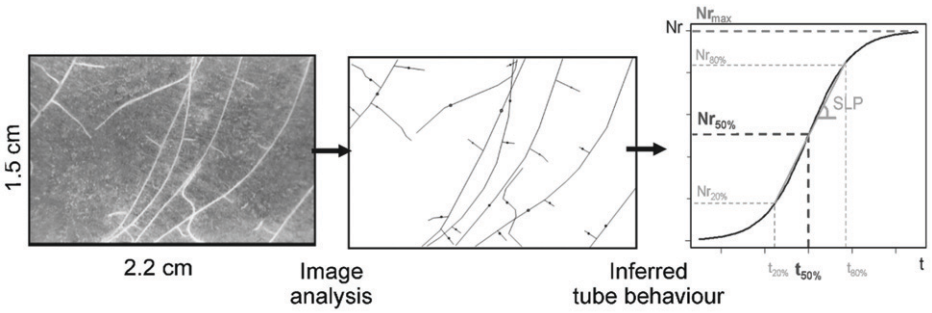

Fig. 2. Minirhizotron image and scheme of typical image analysis. The circles in the central Fig. represent a single root and its diameter. From the count of circles that represent primary roots, in all images taken in a rhizotube, the normalized number of roots in a rhizotube, Nr_{norm} (cm^{-2}) (Eq. [2]) was calculated. A plot of Nr_{norm} versus time represents a root arrival curve which was characterized by three parameters: $t_{50\%}$, Nr_{Max}, and SLP (see text).

The rhizotubes were made of plexiglas; were 60 cm long and had a diameter of 5.72 cm. A BTC2 video microscope (Bartz Technology Corporation, Carpinteria, CA, USA) was used to monitor the root growth on the outer walls of the tubes. Since the rhizotubes had to be installed in the same vertical plane to minimize the disturbance in the soil column, the upper tubes may have put a "growth shadow" on the lower tubes. To minimize this effect the tubes were separated by at least 25 cm soil, which gives the roots a large free vertical distance as compared to the small area of disturbance of the growth.

In each tube and for each sampling time, ten images were collected (image size: 2.2 cm × 1.5 cm); five at the left side of the tube and five at the same location at the right side of the tube. The images were not adjacent (5 cm apart) and were analyzed with the open source software RootFly (Wells and Birchfield, 2009). Figure 2 shows the principle of the image analysis. In a minirhizotron image, roots were characterized by a line along their course and a circle, representing the root length and the root diameter, respectively. We classified roots observed along the minirhizotrons into primary and secondary roots. Secondary roots were defined as roots that were ramifications of another root in the rhizotron image. Roots that were not ramifications of other roots in the image were identified as primary roots. It should be noted that primary roots that were identified in this way may also be secondary roots that ramified from primary roots outside of the minirhizotron image. The number of circles, together with their label "primary" or "secondary" in an image, is thus the number of primary and secondary roots identified in the image. Only the primary roots were used for further analysis.

Throughout the text, we will adopt the following notation convention: capital letters refer to rhizotube based properties, whereas normal letters refer to single image measures. The number of primary roots in the rhizotube images (nr_j) was extrapolated to the whole rhizotube. $Nr(T_i)$ represents the total number of primary roots in a rhizotube (T_i). For this extrapolation, we assumed that all primary roots passing through a virtual rhizotube volume would be observed if the entire tube would be scanned through a viewing window with the same height as the images we used on the left and right-hand side of the tube (see Fig. 3). Normalizing the number of roots in a rhizotube by the horizontal cross-section of the rhizotube allows comparing data from rhizotubes with different length and/or diameter. The normalized total number of roots in a rhizotube is represented by $Nr_{norm}(T_i)$. If only a part

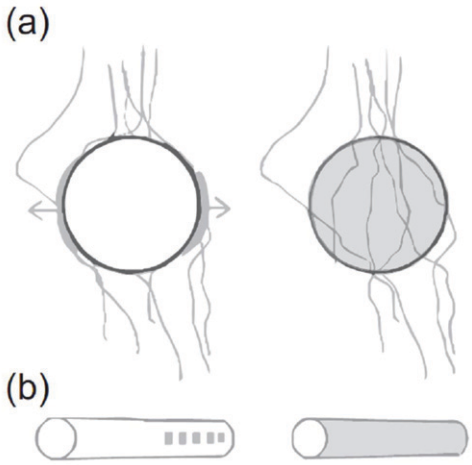

Fig. 3. The normalized virtual growth curves were calculated using two assumptions: (1) (a) the number of roots counted within the volume of a virtual rhizotube equals the number of roots hitting a real rhizotube when observed at the left and the right side of the tube; (2) (b) the total number of roots hitting a rhizotube can be inferred from non-adjacent rhizotube images with a limited range.

of the tube length is scanned by images at the two lateral sides of the tube, the horizontal cross-section that is scanned, $A_{\text{cross,scan}}$ is:

$$A_{\text{cross,scan}} = D\frac{\sum_{N} b_j}{2} = R\sum_{N} b_j \quad [1]$$

where D and R are the tube diameter and radius, respectively, b_j is the width of the jth minirhizotron image along the tube, and N the number of images taken in one tube. The inferred normalized number of roots ($\text{Nr}_{\text{norm}}(T_i)\ L^{-2}$) for a rhizotube T_i is:

$$\text{Nr}_{\text{norm}}(T_i) = \frac{\sum_{N} nr_j}{A_{\text{cross,scan}}} \quad [2]$$

where nr_j the number of roots counted in image j. The effect of measurement uncertainty on this extrapolation approach is discussed in the section Measurement Uncertainty of this paper.

The evolution of $\text{Nr}_{\text{norm}}(T_i)$ with time represents a root arrival curve of primary roots at a certain depth and is therefore, unlike observations of the root growth rate along the soil-rhizotube interface, hardly influenced by disturbances and altered conditions at the soil-rhizotube interface. One drawback of the horizontal tubes could be that, depending on the soil characteristics, water could accumulate on top of the rhizotube during drainage (Philip, 1989). The root growth in the neighborhood of the tube might be affected by such a zone with increased soil moisture content. However, we think that even if this zone occurred in our experiments, it must have been very small, since it didn't show up in the electrical resistivity tomography (ERT) measurements conducted simultaneously with the minirhizotron observations (see Garré et al., 2011). ERT measures water content in the decimeter scale. The root arrival curve may therefore be considered as a robust measure of root growth since the only assumption made is that the observation windows are representative of the whole tube and observation depth. The sigmoid arrival curve of the number of primary roots at each tube, $\text{Nr}_{\text{norm}}(T_i) = f(t)$, was characterized using three parameters: the time for 50% of the final primary root number to be reached ($t_{50\%}$), the maximal amount of primary roots intercepted by each tube (Nr_{Max}) and the slope of the arrival curve between $t_{20\%}$ and $t_{80\%}$ (SLP) (see Fig. 2).

Root System Architecture Model

We used the model RootTyp (Pagès et al., 2004) to simulate the root system architecture of spring barley in the lysimeters. For a comprehensive description of the model, we refer the reader to Pagès et al. (1989, 2004). The RS of a single plant in this model is extended and branched by a set of root tips taking various states (modeled as root types of order 0, 1, 2, etc.). Each root tip extends an axis (axial growth) and can develop lateral axes, called ramifications (branching). Figure 4 shows how the root system is modeled in RootTyp.

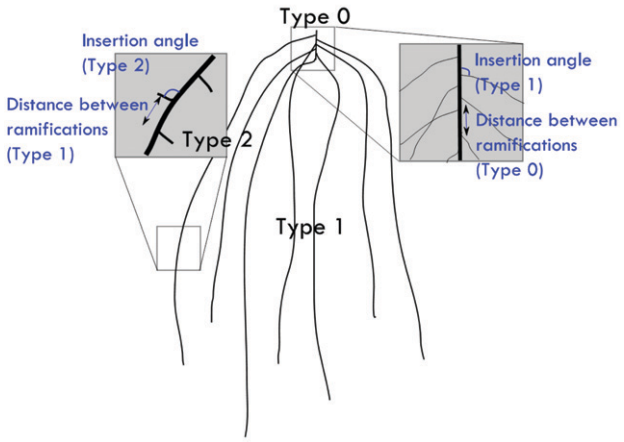

Fig. 4. Scheme of root system built by a set of root tips taking various states as in RootTyp.

The root system starts with a small segment of type 0, representing the base of the shoot system. This segment initiates a certain amount of ramifications (Nr_{Prim}), which is defined by the length of this segment and the distance between the ramifications. These ramifications represent the primary roots. The growth velocity and length of the zeroth order segment, together with the distance between the ramifications control the emission rhythm of the primary roots. For cereals, the emission generally starts a few days after the germination and may continue until flowering (Picard et al., 1985; Wahbi and Gregory, 1995; Doussan et al., 2003; Dupuy et al., 2010b).

The initial direction of a root branch or ramification is defined by two angles: an insertion angle (α) in the common plane defined by the carrying segment and the branch root and a radial angle defined in the plane perpendicular to the carrying segment. The radial angle is drawn at random in a uniform distribution between 0 and 2π. The insertion angle of the ramifications (α) is drawn from the normal distribution with mean $<\alpha>$ and std(α). The root segments grow according to

$$l = l_{\max}\left[1 - e^{-v_{\text{init}}(a/L_{\max})}\right] \quad [3]$$

l, the length of the root; a, the age of the root; $l_{\max}$, the asymptote of the root length and v_{init}, the initial root growth velocity. For a certain root type, v_{init} and $l_{\max}$ are drawn from normal distributions with mean $<v_{\text{init}}>$, $<l_{\max}>$ and standard deviations std(v_{init}), std($l_{\max}$). If $l_{\max}$ is set to a large value (several meters) as is done in this study, Eq. [3] becomes a linear function. At each time step, the growth direction of a root tip is updated. Processes like root elongation, growth direction and branching density are known to be dependent on the soil and the root tips can therefore also interact with it.

Experimental Results

Root Growth of Barley in the Lysimeters

Figure 5 shows the measured arrival curves of the primary roots in S1 and S2 at tube 1 to 4 (T1-T4) with T1 the tube closest to the soil surface. The characteristics ($t_{50\%}$, Nr_{Max}, SLP) of the arrival curves are indicated in Fig. 5 and given in Table 1. The crops have a slightly different growth behavior in S1 than in S2. There is an important difference between S1 and S2 concerning the maximum number of roots at T1, T2, and, most of all, at T3. The lower number of roots in T3 of S1 might be due to the elevated salt ($CaCl_2$) concentration in this lysimeter. However, it must be noted that due to the previous experiments, the conditions in the two soil columns are different so that the root growth curve between the two lysimeters is expected to different. They cannot be considered as replicates. In S2, the roots also reach the deepest horizon quicker than in S1. The effective growth velocity ($v = z/t_{50\%}$), derived from the root arrival curves for a rhizotube at depth z, was between 1.1 and 1.6 cm d^{-1} in S1, whereas v was between 1.4 and 2.6 cm d^{-1} in S2. This effective growth velocity was slightly different for different depths. In soil column S1, the slopes of the arrival curves were not equal for all depths, whereas in S2, they were nearly constant with depth. However, it must be noted that the temporal resolution of the rhizotube observations is rather low so that the uncertainty of the slope of the arrival curve is rather high.

At the end of the growing season, the number of primary roots was the highest at tube 2 (−47.5 cm) in S1 and at tube 3 (−72.5 cm) in S2 (see Fig. 6). Only very few roots reached the last tube at −122.5/-119.5 cm (S1/S2, respectively). The number of primary roots in the first tube was very low in both lysimeters. During the whole growing season, the moisture content increased with depth. As no irrigation was applied, the topsoil dried out and the difference in volumetric soil water content between the bottom and the top of the lysimeter became large (around 0.20 at the end of the experiment. Garré et al. (2011) showed with electrical resistivity tomography measurements that the standard deviation of soil moisture was between min 0.01 and max 0.04 over time in the column S2 (see Fig. 6, 7, and 8, of the paper). The variability was also different for different horizons and ranged over time between 0.02–0.03 in the Ap, between 0.02–0.04 in the Bt and between 0.005–0.015/0.02–0.03 in the Bv1/2. The total water loss due to evapotranspiration during the experiment was highest in S2 (177.7 l). S1 lost 134.2 L water.

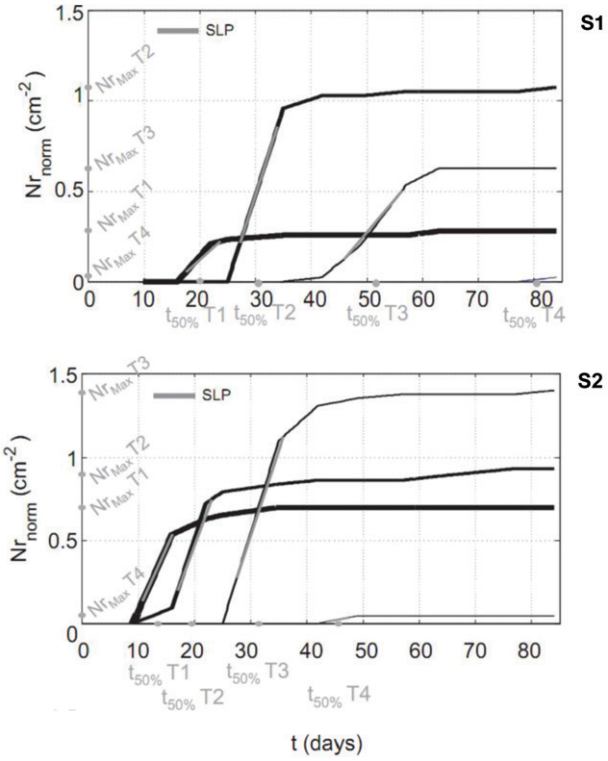

Fig. 5. Normalized measured arrival curves of primary roots for (top) S1 and (bottom) S2 at rhizotubes T1, T2, T3, and T4. The following arrival curve characteristics are shown: $t_{50\%}$, Nr_{Max}, and SLP.

Implications of the Observations

If we summarize the observations, three important observations appear:

1. The highest number of roots was not observed at the tube nearest to the soil surface. This implies that new long roots should originate deeper in the soil profile, provided that the observed root arrival curves are representative for the arrival curve at a certain depth (see later). Primary roots may develop secondary roots much longer than the normal ramifications. These extended secondary roots then behave almost like primary roots and can even develop ramifications of the third order.

Table 1. Arrival curve characteristics in all tubes (T) of lysimeter S1 and S2. $t_{50\%}$ = time at which 50% of the maximal amount of roots has arrived, Nr_{Max} = normalized maximal amount of primary roots seen at the tube, SLP = slope of the arrival curve between $t_{20\%}$ and $t_{80\%}$, v = effective root growth velocity.

	S1				S2			
	T1	T2	T3	T4	T1	T2	T3	T4
$t_{50\%}$ (d)	20	30.5	51.5	80.5	13.5	19.5	31.5	45.5
Nr_{Max} (cm^{-2})	0.28	1.07	0.63	0.02	0.70	0.93	1.40	0.05
SLP (cm^{-2} d^{-1})	0.028	0.096	0.036	0.003	0.063	0.091	0.102	0.006
$v = z/t_{50\%}$ (cm d^{-1})	1.1	1.6	1.4	1.5	1.4	2.3	2.2	2.6

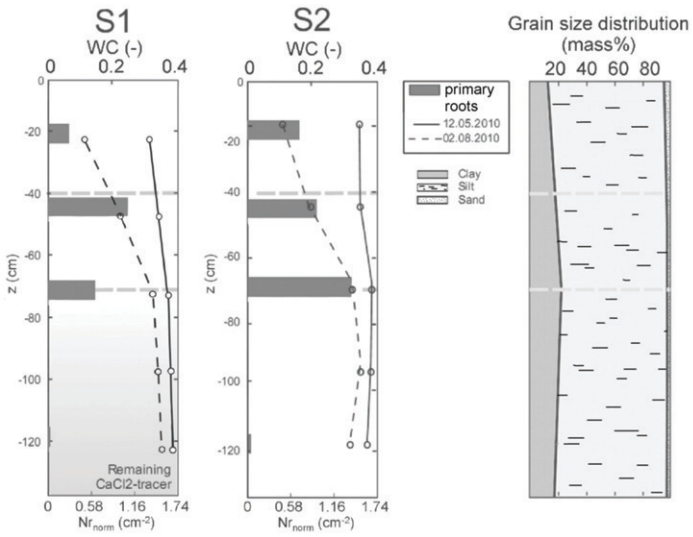

Fig. 6. Measured normalized total number of roots (Nr_{norm}) per rhizotube at the end of the growing season and water content (WC) profiles at 12.05.2009 (DOY 132) and 02.08.2009 (DOY 214) and grain size distribution of the soil at the Merzenhausen field site (Weihermüller, 2005). The boundaries of the soil horizons are indicated with gray dashed lines.

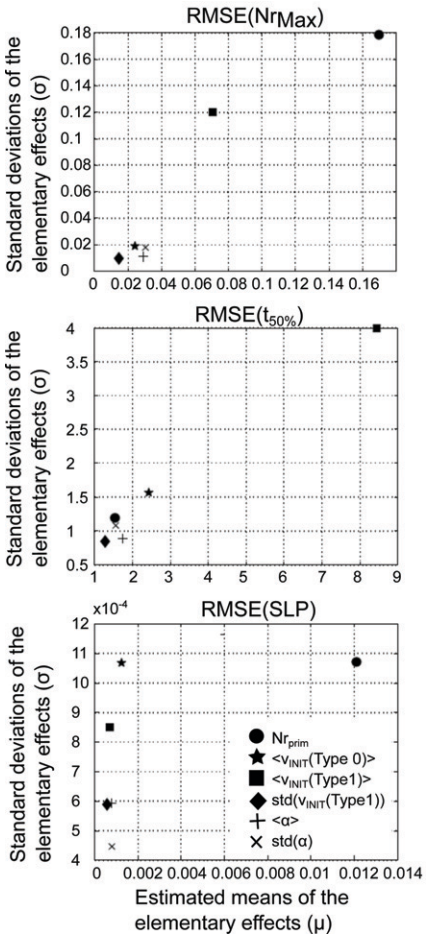

Fig. 7. Results of Morris OAT-test: mean and standard deviation of the elementary effects of six RootTyp model parameters on three curve characteristics: Nr_{Max}, $t_{50\%}$, and SLP.

This process is called reiteration. It is an alternative form of branching, leading simultaneously to axis growth cessation and to production of a number of axes (of the same type) in sub-apical position. Thus, the reiteration process replaces a given root tip with several root tips of the same type (Pagès et al., 2004). Little is still known about the origin of this transformation, but a few publications report the presence of reiteration (Lyford, 1980; Coutts, 1987; Atger and Edelin, 1992; Vercambre et al., 2003). As the surface soils and subsoils are drying at different rates the primary roots in that region may have branched and perished as reported by Rasse et al. (2000) and Pietola and Smucker (1995). Unfortunately, we could not make a vertical section of the lysimeters to observe the whole rooting profile, but there is evidence that this process takes place with barley. Dupriez (2010) followed the root growth of many barley plants in a 2-D rhizotron filled with a homogenous soil (50 × 100 × 0.4 cm^3). They observed a large variability of the root system architecture between plants and regularly saw secondary roots becoming very long and producing ramifications. The experiments of Dupriez (2010) were done under different conditions than the ones in the experiment presented in this paper, but they indicate that the process of reiteration may occur with barley.

2. The effective growth velocity of the roots changes with depth, which may indicate that the layered soil environment causes the roots to change their growth velocity or the tortuosity of their paths within certain horizons. Such behavior can be simulated in the RS architecture model RootTyp by assigning distinct soil layer with different resistances to growth. The observations of changing growth velocity are consistent with the discussion of Dupuy et al. (2010b) on the meristematic waves observed for barley in large, filled containers. Their experiment indicated for example that the time required to reach maximum meristematic activity of barley increases with depth.

3. The slope of the arrival curves changes with depth in one lysimeter (S1). This may again be explained by the possibility of reiteration at some depths, by a changing root growth velocity depending on changing characteristics of the soil horizons or a combination of both. However, the time resolution of the root arrival curves must be high enough to allow an accurate estimation of the slope. The fact that changing slopes do not occur in lysimeter S2 indicates that the cause is not only or entirely soil-specific, since the two soil columns are taken from the same field.

Modeling Results and Optimization

From Root Arrival Curves to Root Architecture Parameters

Combining observed root arrival curves and root architecture modeling, we will address the following questions: "Which parameters of the root growth model RootTyp may be derived from root arrival curves that are observed at different depths using minirhizotron images?" and "What can we learn about the root growth in the two lysimeters from an optimized RS architecture model based on observed root arrival curves?" The first question is directly linked to the way different parameters of the root development model

influence characteristics of the root arrival curves and the change of these characteristics with depth. The second question relates to what the parameters tell us about the root system. To address both questions, we simulated an ensemble of seven rows of barley plants with a distance between the rows of 24 cm. The individual barley plants were equally spaced in the row and the distance between two plants was 2 cm. This corresponds to the distribution in the real lysimeters with the counted number of plants and assumed that all plants were equally distributed over the rows. The total number of plants is 427. For a specific simulation, a parameter set was drawn from the specified parameter distribution for each individual plant. This results in an ensemble of slightly different individual plants.

The model performance was evaluated by comparing the characteristics of the measured arrival curves with those of the "virtual" root arrival curves at virtual rhizotubes at the same location as in the real monoliths. We assume that the possible influence of the tube on the root arrival curves can be neglected and that the observations in the limited number of images are representative for the entire depth. The validity of the second assumption was evaluated conducting virtual sampling with virtual rhizotubes in the simulation. This test allowed us to estimate the uncertainty of the measured root arrival curves (see later). The validity of the first assumption could not be checked formally in this study.

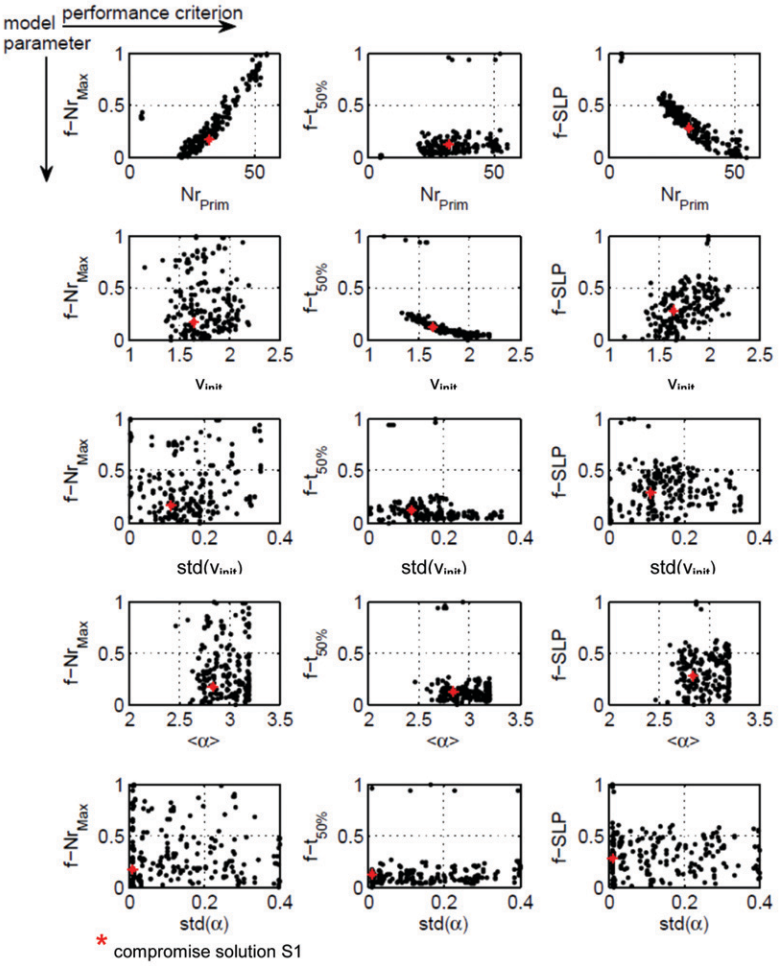

Fig. 8. Performance of the 50 best compromise simulations on the three optimization criteria ($f\_t50\%$, f_Nr_{Max}, f_SLP) as a function of five parameter ranges ($<v_{init}>$ (cm d^{-1}), Nr_{Prim} (-), std(v_{init}) (cm d^{-1}), $<\alpha>$ (rad) and std(α) (rad)) for lysimeter S1.

Model Sensitivity

The sensitivity of the root arrival curves to parameter changes in the RootTyp model was investigated using the Morris One-at-a-time test (Hsu, 1996) and the Eikos MATLAB toolbox. This screening technique is used to compute the local changes of the output due to changes of model parameters. The data analysis is based on elementary effects (EE), which means that the method looks at changes in the output as an effect of changes in a particular model parameter. The Morris method indicates if the effect is negligible, linear or nonlinear or if the considered parameter is involved in interactions with other parameters. A detailed description of this technique can be found in Morris (1991) and Hsu (1996). The model is run for a set of parameter vectors, which is drawn within given parameter ranges. Subsequent parameter vectors in the set differ in only one parameter and different parameters are changed subsequently so that effect of a single parameter change can be evaluated throughout the parameter space. The change in the model output between the two parameter vectors which is due to the change of one individual parameter is called an elementary effect for that changed parameter. From the set of EE's for a specific parameter, the mean of the absolute value and the standard deviation of the EE's are calculated. The mean value of the EE's is a measure for the sensitivity, and their standard deviation is a measure of the nonlinearity of the model in this parameter and the interaction of this parameter with other parameters.

We examined the effect of six parameters on the characteristics of the arrival curves: $<v_{init}(\text{Type 0})>$, $<v_{init}(\text{Type 1})>$, std($v_{init}$(Type 1)), $<\alpha>$, std(α) and Nr_{Prim} with a total number of 70 model evaluations. The minimum and maximum values of these parameters are given in the following two vectors, respectively, in the same order as above: [0.04, 2, 0.01, 2.4, 0.0025, 10] and [0.1, 7, 0.15, 2.9, 0.1, 55]. The sensitivity analysis was performed independently from the optimization. Figure 7 shows the results of the Morris One-at-a-time (OAT) test for the three curve characteristics ($t_{50\%}$, Nr_{Max}, SLP). For each characteristic, the mean and standard deviation of the EE of six different parameters are shown. For Nr_{Max}, the means and standard deviations of the EE are in the same range. The biggest mean effect comes from Nr_{Prim}, followed by the $<v_{init}>$ of the primary roots. This indicates that these two parameters have an important overall influence on Nr_{Max}. For both parameters, the standard deviation of the EE is in the same range as the mean of the EE. This points out that the factors are either

interacting with other factors and/or that they have strong nonlinear effects on Nr_{Max}. The standard deviations of the EE on $t_{50\%}$ are approximately half of the mean of the EE for all parameters under consideration, pointing out interactions with other parameters and/or mildly nonlinear effects. The biggest mean effect on $t_{50\%}$ comes from $<v_{init}(\text{Type 1})>$ and a smaller contribution comes from $<v_{init}(\text{Type 0})>$. The Morris OAT test for SLP reveals that the Nr_{Prim} has the biggest effect on the slope of the root arrival curve. The next biggest overall effect, $<v_{init}(\text{Type 0})>$, is considerably smaller than the one of Nr_{Prim}. However, as compared to Nr_{Prim}, the ratio of the standard deviation and the mean of the EE $<v_{init}(\text{Type 0})>$ is larger, indicating a stronger nonlinear effect or more interaction with other parameters. To summarize, we can state that the parameters Nr_{Prim}, $<v_{init}(\text{Type 1})>$ have the biggest influence on the shape of the root arrival curves. $<v_{init}(\text{Type 0})>$ influences $t_{50\%}$ and SLP to a lesser extent. The influence of the other parameters is much less prominent.

Optimization Strategy

The optimization of the RS architecture model was limited to the following parameters: Nr_{Prim}, $<v_{init}>$, $\text{std}(v_{init})$, $<\alpha>$ and $\text{std}(\alpha)$. The parameter ranges were set encompassing values extracted from literature (Bragg et al., 1984; Hansson and Andrén, 1987; Hansson et al., 1992; Heeraman et al., 1993; Bingham and Bengough, 2003; Kohl et al., 2007; Hargreaves et al., 2009; Dupuy et al., 2010b). The parameter range for Nr_{Prim}, $<v_{init}>$, and $\text{std}(v_{init})$ were respectively set between 5 and 70, 0.5 and 7 cm d^{-1} and between 0.005 and 0.35 cm d^{-1}. The parameter intervals for $<\alpha>$ and $\text{std}(\alpha)$ in radians were [2.35,3.20] and [0.01, 0.4], respectively. The emission of primary roots ($v_{init}(\text{Type 0})$) was considered as known and not included in the optimization process. We assumed that 5 d after germination the primary roots started being emitted and the emission continued until 22 d after germination. These values lie within the time span we can expect for cereals (Picard et al., 1985; Wahbi and Gregory, 1995; Doussan et al., 2003; X. Draye, personal communication, 2011). The parameters which were fixed for all simulations are: the growth velocity of the type 0 root axis (=first axis in the root segment hierarchy), the type of tropism and its intensity, the sensitivity to mechanical resistance, life time of the roots and the probability of transformation of a root (all parameters for the simulations are available on request from the corresponding author). The maximum length (l_{max}) of the primary roots in the model was set very large (10 m) to let them grow at a constant rate during the whole growing period.

We defined three error functions (f) between modeled and observed characteristics of the arrival curves: $t_{50\%}$, Nr_{Max}, and SLP. The use of multiple error functions allowed us to separate the effect of parameters on different characteristics of the root arrival curve. The performance criterion for $t_{50\%}$ is given below as an example:

$$f\_t_{50\%}(\theta) = \sqrt{\sum_{i=T1}^{T4} (t_{50\%}(T_i,\text{simulated}) - t_{50\%}(T_i,\text{measured}))^2} \quad [4]$$

with θ a given parameter set. We adopt a multi-objective optimization framework for two reasons: (i) to better understand the tradeoffs between the different parameters and (ii) to identify a set of parameter combinations satisfying the different performance criteria we defined. We used the AMALGAM code of Vrugt (2006) and Vrugt et al. (2007), which has been found to perform well across a wide range of problems (e.g., Laloy and Bielders, 2009; Huisman et al., 2010). The algorithm operates by defining several performance criteria (=objective functions) that reflect the different characteristics of the root arrival curves. AMALGAM uses a multi-criteria optimization method to identify the range of optimal solutions. These solutions are called Pareto solutions. They represent tradeoffs among the different incommensurable and often conflicting objectives. A set of Pareto solutions has the property that moving from one solution to another, results in the improvement of one objective while causing deterioration in one or more others. The multi-objective inverse problem for this paper can be expressed as:

$$\min_{\theta\in\Theta} F(\theta) = \begin{bmatrix} f\_Nr_{Max}(\theta) \\ f\_t_{50\%}(\theta) \\ f\_\text{SLP}(\theta) \end{bmatrix} \quad [5]$$

where $f\_Nr_{Max}(\theta)$, $f\_t_{50\%}(\theta)$ and $f\_\text{SLP}(\theta)$ are the objective functions related to the arrival curve characteristics Nr_{Max}, $t_{50\%}$, and SLP. The solution to this problem will not be a single "best" parameter set but will consist of a Pareto set $P(\Theta)$ of solutions in the feasible parameter space Θ corresponding to various tradeoffs among the objectives. Because of conflicting demands, it is usually not possible to find a single point θ at which all of the criteria have their minima. In the current case, the "compromise solution," which is the data point closest to the origin of the objective functions scaled by their minimum and maximum, is seen as the optimal solution, as it is more important to match fairly well all characteristics of the arrival curves than to match one very nicely but completely failing to fit the others. In total, we conducted 30,000 forward runs for each optimization run.

Comparing the "simple" root system architecture with the real data shows if the simple model encompasses the processes determining the root architecture development. Although it is impossible to derive a unique parameter combination from the data if we include extra processes in the model and make it more complex, the minirhizotron data give indications on which processes should or should not be considered in a more complex model even if we are not yet able to constrain all parameters with the root arrival data only.

Optimization Results

We concentrate here on the simulation performance for S1, but exactly the same procedure was followed for S2. Figure 8 shows the influence of the different parameter combinations of all

simulated cases on the arrival curve characteristics $t_{50\%}$, Nr_{Max}, and SLP. The rows of Fig. 8 correspond to different parameters, whereas the columns of Fig. 8 correspond to the curve characteristics. The compromise realization is indicated with a red star. Figure 9 shows the objective space of the 50 best compromise realizations of the Pareto set of solutions. The number of primary roots ($<Nr_{Prim}>$) affected mainly the maximum number of roots counted at the rhizotube (Nr_{Max}). This was clear from Fig. 7 and is also visible in the first row of Fig. 8, which shows that for a changing Nr_{Prim}, the f_Nr_{Max} is much more affected than the other criteria. $f_$SLP was also affected by Nr_{Prim}. Just like the sensitivity analysis pointed out, the second row of Fig. 8 shows that the root growth velocity (v_{init}) influences mainly the moment at which 50% of the roots have arrived at a certain depth ($t_{50\%}$). The influence of std(v_{init}) was not as clear as for the other parameters, confirming the low sensitivity of the modeled data to this parameter. As Fig. 8 shows, there was no big difference between the simulated insertion angles and no obviously superior std(α) was found.

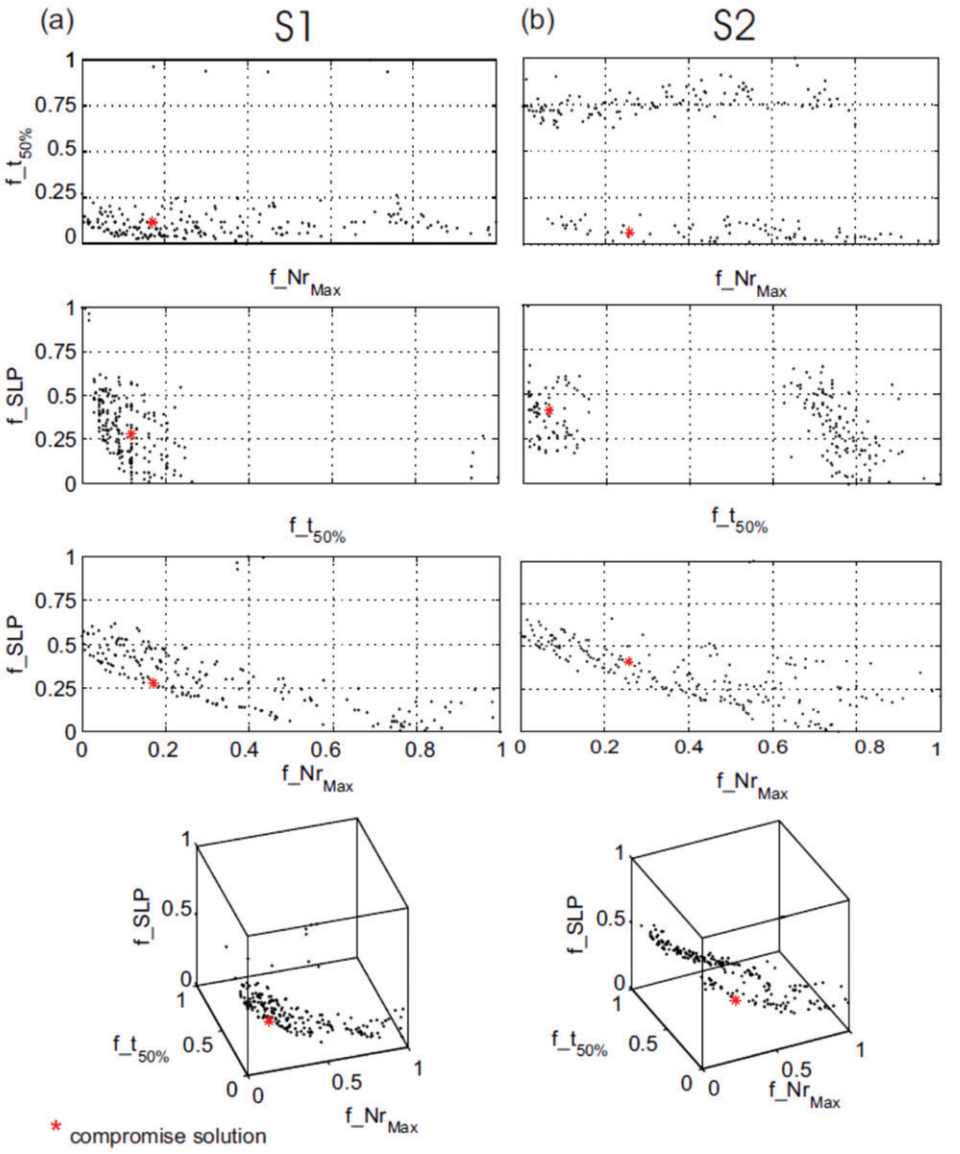

Fig. 9. Two- and three-dimensional projections of the objective space of the Pareto set of solutions for lysimeter (a) S1 and (b) S2. The compromise solution is indicated by the red asterisk.

The best realization, which we defined as the compromise solution, for S1 using a simple root model proved to be $<\alpha> = 2.84$, std(α) = 0.01, $<v_{init}> = 1.65$ cm d^{-1}, std(v_{init}) = 0.11 cm d^{-1}, and $Nr_{Prim} = 31$. Figure 10a shows the simulated and measured arrival curves at the rhizotubes (T1-T4) of S1. The following parameters were best for S2: $<\alpha> = 3.06$, std(α) = 0.0182, $<v_{init}> = 6.4$ cm d^{-1}, std(v_{init}) = 0.0088, and $Nr_{Prim} = 53$. Figure 10b shows the simulated and measured arrival curves of S2. First, these images show that the simple RS model cannot predict the increase in Nr_{Max} with depth. Second, the model over predicts the root growth at greater depths and this leads to unrealistically large rooting depths. A plausible explanation for the latter observation might be preferential growth along the lysimeter walls, potentially causing a higher number of roots and an earlier arrival of roots at certain depth close to the lysimeter walls and vice versa for the number of roots and arrival times observed in the middle of the lysimeter. Since our measurements were collected toward the center of the lysimeter, preferential growth along the lysimeter walls would lead to a decrease of the observed number of roots with depth in the middle of the lysimeter, i.e., the opposite to what we observed. It should be noted that the root growth model predicts a diameter of the root system of a single plant of about 40 cm (see Fig. 11). Given the horizontal dimension of the lysimeter (i.e., 112 cm), the effect of the lysimeter walls on root systems of plants grown in the middle of the lysimeter could therefore be considered as less important. Finally, we checked for preferential root growth by positioning the minirhizotron camera at the lysimeter wall and could not observe earlier root arrival or root accumulation at the lysimeter walls. Based on this, we consider it unlikely that the lower root length densities observed in the deepest minirhizotube than the densities predicted by the root growth model can be explained by preferential growth along the lysimeter walls.

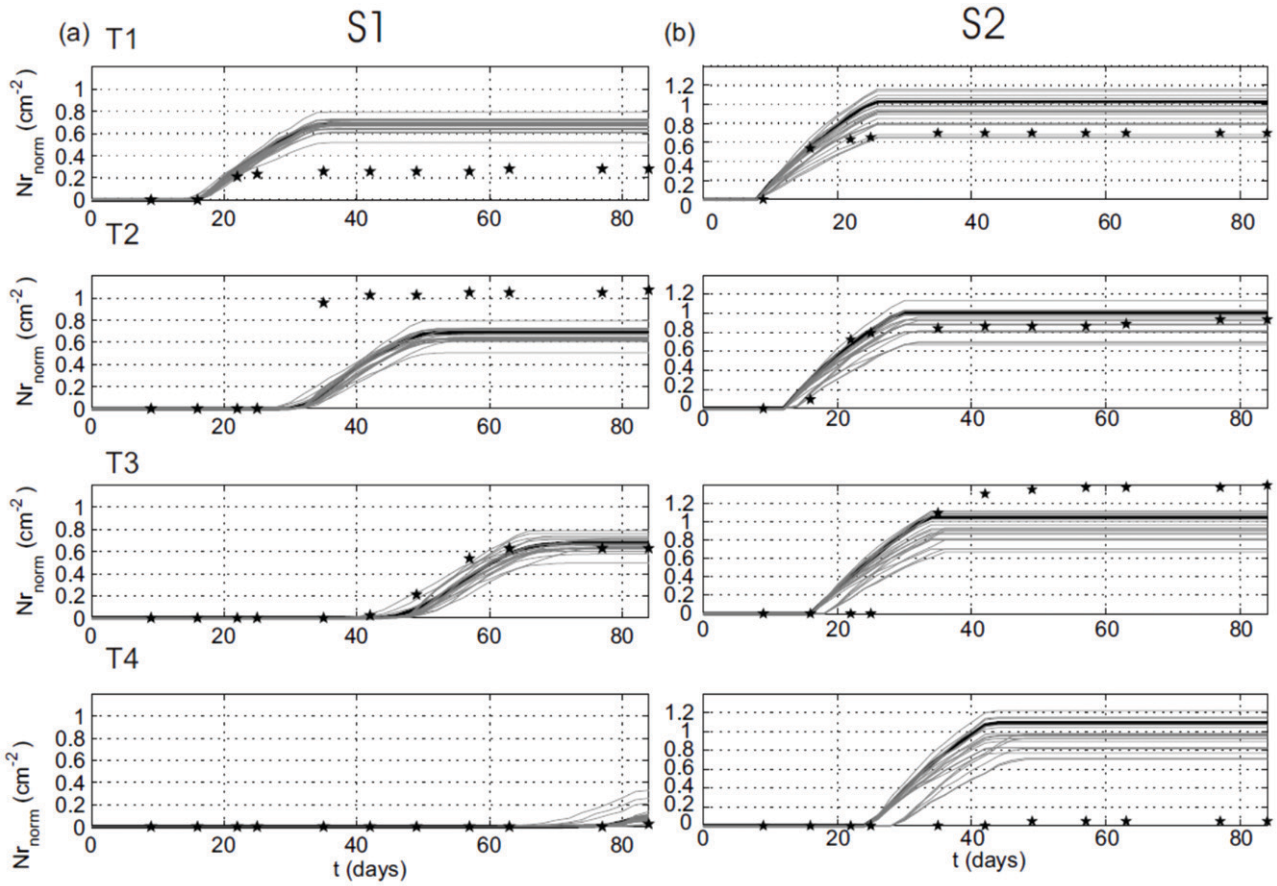

Fig. 10. Normalized simulated (lines) and measured (stars) arrival curves for tubes T1– T4 in (a) lysimeter S1 and (b) lysimeter S2. The lines are the 20 best compromise solutions among the simulations of the pareto front. The black line represents the compromise solution for S1 and S2.

Toward a More Detailed Model

We observed a higher number of roots at −47.5/-44.5 cm depth than at −22.5/-19.5 cm depth. In S2, the number even still increased at −69.5 cm depth. We also observed that the slope of the arrival curves in S1 changed with depth whereas in S2 these slopes were similar in all depths. A simple RS architecture model with a certain amount of primary roots could not reproduce these observations. The simple RS architecture model over predicts the number of roots in the top soil a little and the rooting depth and the number of roots in the deeper soil very strongly. It also inherently has a constant slope of the arrival curves with depth, which is not in agreement with the observations. The simple model with long primary roots growing at a constant velocity in each soil horizon does thus not reproduce the measured root arrival curves. The data suggested two additional processes which may be important to take into account: root reiteration and the influence of stochastic and structural soil heterogeneity.

If we simulate root growth with the possibility of a reiteration process, which replaces a given root tip with several root tips of the same type, it is possible to increase the root number with depth and to obtain variable slopes of the arrival curve with depth. However, this increases the number of parameters to be optimized with four: a date at which the reiteration starts, a probability for the reiteration to take place and a minimum and maximum number of roots to be formed at the root tip when it re-iterates. Using only minirhizotron data, it is impossible to estimate a unique parameter set, since there is no information on the origin of the roots arriving at the rhizotube. Such information may be retrieved from experiments in 2D-rhizoboxes filled with comparable soil material or using MRI imaging in long soil cores.

The soil, conceptualized as an ensemble of horizontal layers, can affect root elongation and direction (e.g., Barley, 1962; Bengough et al., 2006), as well as root branching density (Goss, 1977). Its influence is formalized in the model RootTyp using simple coefficients representing the soil constraint and the sensitivity of a certain root type to this constraint. Again, this adds many unknown parameters to the model which cannot be estimated using minirhizotron data alone. Even if the soil density and moisture content are known, the reaction of primary and secondary roots on their environment remains largely unknown, since an undisturbed, natural soil is heterogeneous. However, from the shape of the different arrival curves, the very low number of roots at the bottom and the changing effective growth velocities, it becomes clear that the soil must have influenced the root development and as such, the minirhizotron

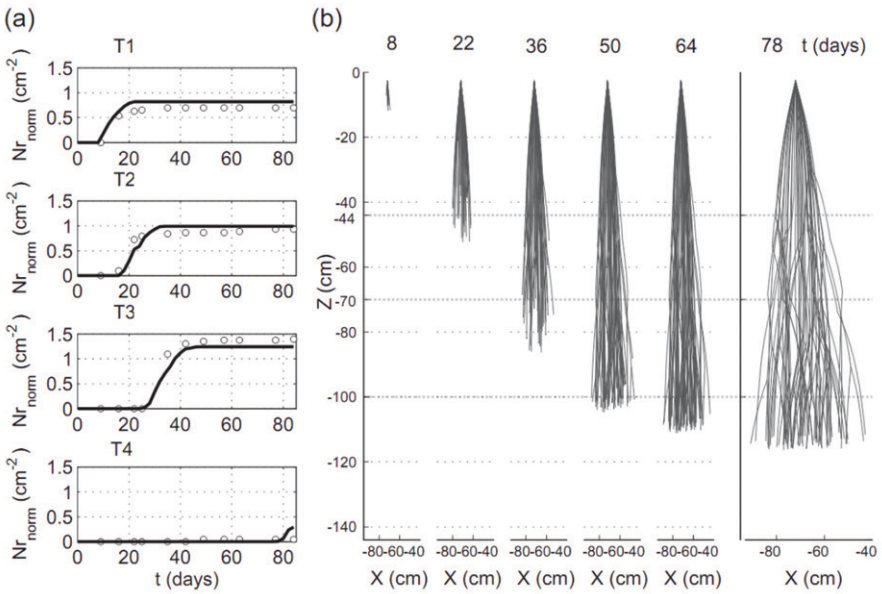

Fig. 11. (a) Normalized simulated (complex model) and measured arrival curves for tubes T1– T4 in lysimeter S2; (b) evolution in time of the simulated complex root system with reiteration and soil layering for lysimeter S2. The gray dashed lines indicate the soil horizon boundaries.

data do provide important information to formulate hypotheses for a better root architecture model. Separate experiments in small, undisturbed samples of the different soil horizons may elucidate the influence of the soil on root growth velocity using non-invasive techniques like radiography.

Figure 11a shows the simulated and measured root arrival curves of lysimeter S2 using a complex model with reiteration and soil layering (decreased root growth velocity in the B_{v2} horizon). Figure 11b depicts the root system of a single plant in the simulation. This solution fits the data much better than the optimal simple RS model; however, the solution is not unique. For instance, defining other thicknesses of layers with a different resistance to root growth would lead to other parameterizations but reproduce the same fit. Nevertheless, the minirhizotron data indicate that reiteration and soil influences should be taken into account.

Measurement Uncertainty

An important prerequisite for the calibration approach we presented is that the dataset is reliable, representative, and accurate. It is therefore necessary to assess the uncertainty on the measured mean tube behavior based on ten minirhizotron images. In our study, this could not be tested using the data themselves directly, as we did not have repetitions of the minirhizotron measurements at other places in the lysimeter at the same depth. Additionally, the data are expected to be spatially correlated, which makes it impossible to use the variance between individual images to estimate the variance of the mean. However, the uncertainty can be investigated using a so-called simulation experiment. We assume that the root growth can be described by the RS architecture model and model parameters that we derived. Then this model is used to generate a set of measurements and discuss the uncertainty or variability of the statistic (the cumulative root arrival curve) which is derived from these simulated measurements. Using a spatial analysis of stochastically simulated root systems, we can assess the variability and the uncertainty on the mean number of roots obtained from our measurement setup.

We divided a virtual soil column equal to the real lysimeters in a mesh with cells of dx = 1.5 cm, dy = 5.72 cm, and dz = 5.72 cm, where dx corresponds to the width of an image and dy and dz represent the diameter of the minirhizotron. Each cell represented a couple of minirhizotron images at the left and the right side at one location in the tube. To mimic the real measurements, we took n sample sets containing always five of these cells with a distance of 5 cm between the cells. For each sample i, a local mean (μ_i) of the number of roots can be calculated. The global mean M was calculated for n possible samples in the soil column. The uncertainty of M with the chosen sampling design was estimated by calculating the variance of the local μ_i. In a first analysis, the sample sets always had the same orientation with respect to the plant rows (i.e., perpendicular) but the set could be located anywhere on the Y-axis. In a second analysis, the sample again had the same orientation with respect to the plant rows (i.e., perpendicular), but also same distance to the rows as in the measurements was considered. The standard deviation of μ_i for both analyses represents an upper (sample sets of 5 × 2 images located randomly on the Y-axis, "unrestricted" standard deviation, STD_{unres}) and a lower boundary (sample sets of 5 × 2 images always with the same distance from the rows, "restricted" standard deviation, STD_{res}) for the variance of the estimated normalized number of roots in the rhizotube.

Table 2 shows these variances and the corresponding means of $<Nr_{norm}>$ for the simulation shown in Fig. 11, 84 d after sowing. At the top the unrestricted standard deviation of the mean is clearly higher than the restricted one, but at the lower depths, this is not the case anymore. In general, the standard deviations are rather high as compared to the mean. This means that it is advisable for future experiments to take more samples. However, for both cases, there is a significant difference between mean number of roots

Table 2. Standard deviations of the mean normalized number of roots (<Nr_{norm}>) for the simulation shown in Fig. 11 if samples of 5 × 2 images are taken anywhere in the column (STD_{unres}) and standard deviation of <Nr_{norm}> if samples of 5 × 2 images are always situated at the same distance to the plant rows (STD_{res}). Both STD_{res} and STD_{unres} have rhizotubes oriented perpendicular to the plant rows.

	$Mean_{res}$ (cm^{-2}), STD_{res} (cm^{-2})	$Mean_{unres}$ (cm^{-2}), STD_{unres} (cm^{-2})
	$n = 60$	$n = 600$
T1: -19.5 cm	1.07, 0.15	1.19, 0.20
T2: -44.5 cm	1.29, 0.18	1.31, 0.20
T3: -69.5 cm	1.65, 0.29	1.69, 0.25
T4: -119.5 cm	0.48, 0.12	0.49, 0.12

in the four tubes according to the Tukey's HSD criterion with a confidence level of 0.05, which means that the number of roots at several depths can definitely be used to parameterize a root system architecture model.

Conclusions

Minirhizotrons are the only way to retrieve dynamic information on root growth and root system (RS) architecture in an undisturbed soil environment at the lysimeter or field scale without destroying parts of the root system. RS architecture model parameters having an important influence on the root arrival curve at a certain depth are: the root growth velocity, the number of primary roots emitted and the mean insertion angle of these roots. Using the global, multi-objective optimization algorithm AMALGAM, we estimated these parameters to fit the minirhizotron data at four depths in an undisturbed soil monolith. The deviation between the model results and the observations indicated that other processes which were not considered in the simple simulations, such as reiteration, played an important role in the root development during this experiment. It must be noted that the experiments were run under extreme conditions (i.e., no rain or irrigation during the entire growing season and remaining salt tracer at the bottom of one of the lysimeters). Processes such as reiteration may therefore be a reaction of the plant to these conditions so as to optimize the water uptake from deeper soil layers.

However, we showed that the minirhizotron technique in this set-up does not provide enough information to restrain a RS architecture model with reiteration and soil layering in a satisfying way. To reduce measurement uncertainty, a large number of minirhizotron images should be made along the tube and with high temporal resolution. Based on these measurements, a geostatistical uncertainty analysis could be performed. Our uncertainty evaluation approach using Monte Carlo simulations could also be used to estimate the uncertainty associated with a certain measurement setup a priori so as to optimize and design minirhizotron measurements. To assess the effect of the soil, the use of more tubes at more depths could increase the information content of the ensemble of growth curves. It should be noted that parameters such as local root growth and insertion angles of secondary roots might not be derived directly from frequent observations of root growth along minirhizotrons since the disturbance of the soil at the rhizotron-soil interface may affect local root growth. To further reduce the number of unknowns, vertical sections of the root system in a trench at the end of an experiment could be used to measure e.g., root insertion angles and the occurrence and location of reiteration. The primary root emission rhythm could be measured at a smaller scale using non-invasive imaging techniques such as MRI as also mentioned by Gregory et al. (2003). Additional information from other experiments on the plant under consideration and in a similar environment is thus necessary and may greatly improve the model results. Nevertheless, even with little information, a simple model with primary roots can be adjusted, making it possible to explore realistic rooting profiles going beyond the limited, discrete measurements of a few rhizotubes. Since many water flow models rely on a root density profile to predict root water uptake, this is of great importance (Draye et al., 2010).

Appendix

α	insertion angle of ramifications (= branches) (rad)
l_{max}	maximum root length (cm)
Morris OAT test	Morris one-at-a-time test (Hsu, 1996)
nr	number of roots in a minirhizotron image
Nr	number of roots in an entire rhizotube
Nr_{max}	maximal amount of primary roots intercepted by a rhizotube
Nr_{norm}	number of roots in an entire rhizotube normalized by the horizontal cross section of the rhizotube (cm^{-2})
Nr_{Prim}	number of primary roots initiated from the initial root axis (Type 0)
S1, S2	Lysimeter 1, Lysimeter 2
T1–4	rhizotube 1–4
$t_{50\%}$	the time for 50% of the final primary root number to be reached
v_{init}	initial root growth velocity (cm d^{-1})

Acknowledgments

We would like to thank Prof. Jasper Vrugt, UC Irvine for the useful comments and the permission to use his computational resources.

References

Atger, C., and C. Edelin. 1992. Premières données sur l'architecture comparée des systèmes racinaires et caulinaires des arbres. Can. J. Bot. 72(7):963–975.

Barley, K.P. 1962. The effects of mechanical stress on the growth of roots. J. Exp. Bot. 13:95–110. doi:10.1093/jxb/13.1.95.

Bengough, A.G., M.F. Bransby, J. Hans, S.J. McKenna, T.J. Roberts, and T.A. Valentine. 2006. Root responses to soil physical conditions; growth dynamics from field to cell. J. Exp. Bot. 57:437–447. doi:10.1093/jxb/erj003.

Bingham, I.J., and A.G. Bengough. 2003. Morphological plasticity of wheat and barley roots in response to spatial variation in soil strength. Plant Soil 250:273–282. doi:10.1023/A:1022891519039.

Bragg, P., G. Govi, and R. Cannell. 1983. A comparison of methods, including angled and vertical minirhizotrons, for studying root growth and distribution in a spring oat crop. Plant Soil 73:435–440. doi:10.1007/BF02184322.

Bragg, P.L., P. Rubino, F.K.G. Henderson, W.J. Fielding, and R.Q. Cannell. 1984. A comparison of the root and shoot growth of winter barley and winter wheat, and the effect of an early application of chlormequat. J. Agric. Sci. 103:257–264. doi:10.1017/S0021859600047201.

Burkhardt, M., R. Kasteel, S. Giesa, and H. Vereecken. 2005. Characterization of field tracer transport using high-resolution images. Vadose Zone J. 4:101–111. doi:10.2113/4.1.101.

Clausnitzer, V., and J. Hopmans. 1994. Simultaneous modeling of transient three-dimensional root growth and soil water flow. Plant Soil 164:299–314. doi:10.1007/BF00010082.

Coutts, M.P. 1987. Developmental processes in tree root systems. Can. J. For. Res. 17:761–767. doi:10.1139/x87-122.

Diggle, A. 1988. ROOTMAP—A model in three-dimensional coordinates of the growth and structure of fibrous root systems. Plant Soil 105:169–178. doi:10.1007/BF02376780.

Doussan, C., L. Pagès, and A. Pierret. 2003. Soil exploration and resource acquisition by plant roots: An architectural and modelling point of view. Agronomie 23:419–431. doi:10.1051/agro:2003027.

Draye, X., Y. Kim, G. Lobet, and M. Javaux. 2010. Model-assisted integration of physiological and environmental constraints affecting the dynamic and spatial patterns of root water uptake from soils. J. Exp. Bot. 61:2145–2155. doi:10.1093/jxb/erq077.

Dupriez, M. 2010. Effets combinés de la croissance racinaire et de la prise d'eau chez l'orge MSc. thesis UCL, Louvain-la-Neuve, France.

Dupuy, L., P.J. Gregory, and A.G. Bengough. 2010a. Root growth models: Towards a new generation of continuous approaches. J. Exp. Bot. 61:2131–2143. doi:10.1093/jxb/erp389.

Dupuy, L., M. Vignes, B.M. McKenzie, and P.J. White. 2010b. The dynamics of root meristem distribution in the soil. Plant Cell Environ. 33:358–369. doi:10.1111/j.1365-3040.2009.02081.x.

FAO/ISRIC/ISSS. 1998. World reference base for soil resources, World Soil Resources Reports. International Society of Soil Science, Rome.

Garré, S. 2010. Non-invasive monitoring of water and solute fluxes in a cropped soil. Forschungszentrum Jülich Zentralbibliothek, Verlag, Jülich, Germany.

Garré, S., M. Javaux, J. Vanderborght, L. Pages, and H. Vereecken. 2011. Three-dimensional electrical resistivity tomography to monitor root zone water dynamics. Vadose Zone J. 10:412–424. doi:10.2136/vzj2010.0079.

Goss, M.J. 1977. Effects of mechanical impedance on root growth in barley (Hordeum vulgare L.). J. Exp. Bot. 28:96–111. doi:10.1093/jxb/28.1.96.

Gregory, P.J., D.J. Hutchison, D.B. Read, P.M. Jenneson, W.B. Gilboy, and E.J. Morton. 2003. Non-invasive imaging of roots with high resolution X-ray micro-tomography. Plant Soil 255:351–359. doi:10.1023/A:1026179919689.

Hackett, C., and D.A. Rose. 1972. A model of the extension and branching of a seminal root of barley, and its use in studying relations between root dimensions. I. The model. Aust. J. Biol. Sci. 25:669–679.

Hansson, A., and O. Andrén. 1987. Root dynamics in barley, lucerne and meadow fescue investigated with a mini-rhizotron technique. Plant Soil 103:33–38. doi:10.1007/BF02370664.

Hansson, A.C., E. Steen, and O. Andrén. 1992. Root growth of daily irrigated and fertilized barley investigated with ingrowth cores, soil cores and minirhizotrons. Swed. J. Agric. Res. 22:141–152.

Hargreaves, C., P. Gregory, and A. Bengough. 2009. Measuring root traits in barley (Hordeum vulgare ssp. vulgare and ssp. spontaneum) seedlings using gel chambers, soil sacs and X-ray microtomography. Plant Soil 316:285–297. doi:10.1007/s11104-008-9780-4.

Heeraman, D.A., P.H. Crown, and N.G. Juma. 1993. A color composite technique for detecting root dynamics of barley from minirhizotron images. Plant Soil 157:275–287. doi:10.1007/BF00011056.

Hsu, J.C. 1996. Multiple comparisons: Theory and methods. Chapman and Hall, London.

Huisman, J.A., J. Rings, J.A. Vrugt, J. Sorg, and H. Vereecken. 2010. Hydraulic properties of a model dike from coupled Bayesian and multi-criteria hydrogeophysical inversion. J. Hydrol. 380:62–73. doi:10.1016/j.jhydrol.2009.10.023.

Kohl, M., U. Böttcher, and H. Kage. 2007. Comparing different approaches to calculate the effects of heterogeneous root distribution on nutrient uptake: A case study on subsoil nitrate uptake by a barley root system. Plant Soil 298:145–159. doi:10.1007/s11104-007-9347-9.

Laloy, E., and C.L. Bielders. 2009. Modelling intercrop management impact on runoff and erosion in a continuous maize cropping system: Part II. Model Pareto multi-objective calibration and long-term scenario analysis using disaggregated rainfall. Eur. J. Soil Sci. 60:1022–1037. doi:10.1111/j.1365-2389.2009.01190.x.

Levan, M.A., J.W. Ycas, and J.W. Hummel. 1987. Light leak effects on near surface soybean rooting observed with minirhizotrons. In: H.M. Taylor, editor, Minirhizotron observation tubes: Methods and applications for measuring rhizosphere dynamics. ASA Spec. Publ. 50. ASA, CSSA, SSSA, Madison, WI. p. 89–98.

Lyford, W.H. 1980. Development of the root system of northern red oak (Quercus rubra L.). Harvard For. Pap. 21, Harvard Univ. Harvard For., Petersham, MA. p. 1–30.

Lynch, J.P., K.L. Nielsen, R.D. Davis, and A.G. Jablokow. 1997. SimRoot: Modelling and visualization of root systems. Plant Soil 188:139–151. doi:10.1023/A:1004276724310.

McMichael, B.L., and H.M. Taylor. 1987. Applications and limitations of rhizotrons and minirhizotrons. In: H.M. Taylor, editor, Minirhizotron observation tubes: Methods and applications for measuring rhizosphere dynamics. ASA Spec. Publ. 50. ASA, CSSA, SSSA, Madison, WI. p. 1–13.

Menon, M., B. Robinson, S.E. Oswald, A. Kaestner, K.C. Abbaspour, E. Lehmann, and R. Schulin. 2007. Visualization of root growth in heterogeneously contaminated soil using neutron radiography. Eur. J. Soil Sci. 58:802–810. doi:10.1111/j.1365-2389.2006.00870.x.

Moradi, A., H. Conesa, B. Robinson, E. Lehmann, G. Kuehne, A. Kaestner, S. Oswald, and R. Schulin. 2009. Neutron radiography as a tool for revealing root development in soil: Capabilities and limitations. Plant Soil 318:243–255. doi:10.1007/s11104-008-9834-7.

Morris, M.D. 1991. Factorial sampling plans for preliminary computational experiments. Technometrics 33:161–174.

Pagès, L., M.O. Jordan, and D. Picard. 1989. A simulation model of the three-dimensional architecture of the maize root system. Plant Soil 119:147–154. doi:10.1007/BF02370279.

Pagès, L., G. Vercambre, J.-L. Drouet, F. Lecompte, C. Collet, and J. Le Bot. 2004. Root Typ: A generic model to depict and analyse the root system architecture. Plant Soil 258:103–119. doi:10.1023/B:PLSO.0000016540.47134.03.

Parker, C.J., M.K.V. Carr, N.J. Jarvis, B.O. Puplampu, and V.H. Lee. 1991. An evaluation of the minirhizotron technique for estimating root distribution in potatoes. J. Agric. Sci. 116:341–350. doi:10.1017/S0021859600078151.

Philip, J.R. 1989. Multidimensional steady infiltration to a water table. Water Resour. Res. 25:109–116. doi:10.1029/WR025i001p00109.

Picard, D., M.O. Jordan, and R. Trendel. 1985. Rythme d□apparition des racines primaires du maïs (Zea mays L.) I.□ Etude détaillée pour une variété en un lieu donné. Agronomie 5:667–676. doi:10.1051/agro:19850801.

Pietola, L.M., and A.J.M. Smucker. 1995. Fine root dynamics of alfalfa after multiple cuttings and during a late invasion by weeds. Agron. J. 87:1161–1169. doi:10.2134/agronj1995.00021962008700060021x.

Pohlmeier, A., A. Oros-Peusquens, M. Javaux, M.I. Menzel, J. Vanderborght, J. Kaffanke, S. Romanzetti, J. Lindenmair, H. Vereecken, and N.J. Shah. 2008. Changes in soil water content resulting from root uptake monitored by magnetic resonance imaging. Vadose Zone J. 7:1010–1017. doi:10.2136/vzj2007.0110.

Rasse, D.P., A.J.M. Smucker, and D. Santos. 2000. Alfalfa root and shoot mulching effects on soil hydraulic properties and aggregation. Soil Sci. Soc. Am. J. 64:725–731. doi:10.2136/sssaj2000.642725x.

Smit, A.L., E. George, and J. Groenwold. 2000. Root observations and measurements at (transparant) interfaces with soil. In A.L. Smit, A.G. Bengough, C. Engels et al., editors, Root methods: A handbook. Springer, Berlin. p. 587.

Somma, F., J.W. Hopmans, and V. Clausnitzer. 1998. Transient three-dimensional modeling of soil water and solute transport with simultaneous root growth, root water and nutrient uptake. Plant Soil 202:281–293. doi:10.1023/A:1004378602378.

Tracy, S.R., J.A. Roberts, C.R. Black, A. McNeill, R. Davidson, and S.J. Mooney. 2010. The X-factor: Visualizing undisturbed root architecture in soils using X-ray computed tomography. J. Exp. Bot. 61:311–313. doi:10.1093/jxb/erp386.

Upchurch, D.R., and J.T. Ritchie. 1983. Root observations using a video recording system in mini-rhizotrons. Agron. J. 75:1009–1015. doi:10.2134/agronj1983.00021962007500060033x.

Vercambre, G., L. Pagès, C. Doussan, and R. Habib. 2003. Architectural analysis and synthesis of the plum tree root system in an orchard using a quantitative modelling approach. Plant Soil 251:1–11. doi:10.1023/A:1022961513239.

Vos, J., and J. Groenwold. 1987. The relation between root growth along observation tubes and in bulk soil. In H.M. Taylor, editor, Minirhizotron observation tubes: Methods and applications for measuring rhizosphere dynamics. ASA Spec. Publ. 50. ASA, CSSA, SSSA, Madison, WI. p. 39–49.

Vrugt, J.A. 2006. Multi-objective calibration of forecast ensembles using Bayesian model averaging. Geophys. Res. Lett. 33:L19817. doi:10.1029/2006GL027126.

Vrugt, J.A., J. Van Belle, and W. Bouten. 2007. Pareto front analysis of flight time and energy use in long-distance bird migration. J. Avian Biol. 38:432–442. doi:10.1111/j.0908-8857.2007.03909.x.

Wahbi, A., and P.J. Gregory. 1995. Growth and development of young roots of barley (Hordeum vulgare L.) genotypes. Ann. Bot. 75:533–539. doi:10.1006/anbo.1995.1055

Weihermüller, L. 2005. Comparison of different soil water extraction systems for the prognoses of solute transport at the field scale using numerical simulations, field and lysimeter experiments. Rheinische Friedrich-Wilhelms Univ., Bonn, Germany.

Wells, C.E., and S. Birchfield. 2009. Rootfly: Software for minirhizotron image analysis. Clemson University, Kingstree, SC.

Willatt, S.T., R.G. Struss, and H.M. Taylor. 1978. In situ root studies using neutron radiography. Agron. J. 70:581–586. doi:10.2134/agronj1978.00021962007000040016x.

Willigen, P.d., M. Heinen, A. Mollier, and M.V. Noordwijk. 2002. Two-dimensional growth of a root system modelled as a diffusion process. I. Analytical solutions. Plant Soil 240:225–234. doi:10.1023/A:1015744529454.

Wu, L., M.B. McGechan, N. McRoberts, J.A. Baddeley, and C.A. Watson. 2007. SPACSYS: Integration of a 3D root architecture component to carbon, nitrogen and water cycling—Model description. Ecol. Modell. 200:343–359. doi:10.1016/j.ecolmodel.2006.08.010.